The Astro-H High Resolution Soft X-Ray Spectrometer

Richard.L. Kelley[*a], Kazuhisa Mitsuda[b] Hiroki Akamatsu[c], Phillipp Azzarell[d], Tom Bialas[a], Kevin R. Boyce[a], Gregory V. Brown[e], Edgar Canavan[a], Meng P. Chiao[a,f], Elisa Costantini[c], Michael J. DiPirro[a], Megan E. Eckart[a], Yuichiro Ezoe[g], Ryuichi Fujimoto[h], Daniel Haas[c], Jan-Willem den Herder[c], Akio Hoshino[i], Kumi Ishikawa[j], Yoshitaka Ishisaki[g], Naoko Iyomoto[l], Caroline A. Kilbourne[a], Mark Kimball[a], Shunji Kitamoto[h], Saori Konami[f], Shu Koyama[l], Maurice A. Leutenegger[a,f], Candace Masters[a], Dan McCammon[m], Joseph Miko[a], , Ikuyuki Mitsuishi[n], S. Harvey Moseley[a], Hiroshi Murakami[o], Masahide Murakami[p], Hirofumi Noda[q], Mina Ogawa[b], Takaya Ohashi[g], Atsushi Okamoto[r], Naomi Ota[s], Stéphane Paltani[d], F. Scott Porter[a], Kazuhiro Sakai[a,t], Kosuke Sato[u], Yohichi Sato[q], Makoto Sawada[v], Hiromi Seta[g], Keisuke Shinozaki[r], Peter J. Shirron[a], Gary A. Sneiderman[a], Hiroyuki Sugita[r], Andrew E. Szymkowiak[w], Yoh Takei[b], Toru Tamagawa[i], Makoto Tashiro[x], Yukikatsu Terada[x], Masahiro Tsujimoto[b], Cor P. de Vries[c], Tomomi Watanabe[a], Shinya Yamada[g], Noriko Y. Yamasaki[b], and Yoichi Yatsu[y]

[a]NASA/Goddard Space Flight Center, Greenbelt, MD 20771 USA
[b]Institute of Space and Astronautical Science (ISAS), Japan Aerospace Exploration Agency (JAXA), Kanagawa 252-5210, Japan
[c]SRON Netherlands Institute for Space Research, Utrecht, The Netherlands
[d]Dept. of Astronomy, University of Genova, Versoix CH-1290, Switzerland
[e]Lawrence Livermore National Laboratory, CA 94550, USA
[f]University of Maryland, Baltimore County, Baltimore, MD 21250 USA
[g]Dept. of Physics, Tokyo Metropolitan University, Tokyo 192-0397, Japan
[h]Faculty of Mathematics and Physics, Kanazawa University, Ishikawa 920-1192, Japan
[i]Dept. of Physics, Rikkyo University, Tokyo 171-8501, Japan
[j]RIKEN Nishina Center, Saitama 351-0198, Japan
[k]Dept. of Physics, Tokyo Metropolitan University, Tokyo 192-0397, Japan
[l]Kyushu University, Fukuoka 819-0395, Japan
[m]Dept. of Physics, University of Wisconsin, Madison, WI 53706 USA
[n]Dept. of Physics, Nagoya University, Aichi 464-8602, Japan
[o]Dept. of Information Science, Faculty of Liberal Arts, Tohoku Gakuin University, Miyagi 981-3193, Japan
[p]Dept. of Architecture, Kindai University, Osaka 577-8502, Japan
[q]Frontier Research Institute for Interdisciplinary Sciences, Tohoku University, Miyagi 980-8578, Japan
[r]Tsukuba Space Center (TKSC), Japan Aerospace Exploration Agency (JAXA), Ibaraki 305-8505, Japan
[s]Dept. of Physics, Faculty of Science, Nara Women's University, Nara 630-8506, Japan
[t]Universities Space Research Association, Huntsville, AL 35805 USA
[u]Dept. of Physics, Tokyo University of Science, Tokyo 162-8601, Japan
[v]Dept. of Physics and Mathematics, Aoyama Gakuin University, Kanagawa 252-5258, Japan
[w]Dept. of Physics, Yale University, New Haven, CT 06520 USA
[x]Dept. of Physics, Saitama University, Saitama 338-8570, Japan
[y]Dept. of Physics, Tokyo Institute of Technology, Tokyo 152-8551, Japan

---

[*] Richard.L.Kelley@nasa.gov

Abstract. We present the overall design and performance of the Astro-H (Hitomi) Soft X-Ray Spectrometer (SXS). The instrument uses a 36-pixel array of x-ray microcalorimeters at the focus of a grazing-incidence x-ray mirror Soft X-Ray Telescope (SXT) for high-resolution spectroscopy of celestial x-ray sources. The instrument was designed to achieve an energy resolution better than 7 eV over the 0.3-12 keV energy range and operate for more than 3 years in orbit. The actual energy resolution of the instrument is 4-5 eV as demonstrated during extensive ground testing prior to launch and in orbit. The measured mass flow rate of the liquid helium cryogen and initial fill level at launch predicted a lifetime of more than 4 years assuming steady mechanical cooler performance. Cryogen-free operation was successfully demonstrated prior to launch. The successful operation of the SXS in orbit, including the first observations of the velocity structure of the Perseus cluster of galaxies, demonstrates the viability and power of this technology as a tool for astrophysics.

Keywords: Detectors, x-rays, calorimeters, spectrometers, instruments, missions

1 Introduction

The Soft X-Ray Spectrometer (SXS) is one of four instruments on the Astro-H observatory (renamed *Hitomi* after successfully reaching orbit on 2016 February 17). It was designed to provide high-resolution x-ray spectroscopy from 0.3-12 keV to addresses a broad range of important astrophysical questions, both on its own and in conjunction with the other co-aligned instruments on the Hitomi X-ray Observatory (Fig. 1)[1]. As a standalone instrument, the SXS design is capable of critical contributions in three of the most important areas of astrophysics: the formation and evolution of galaxies through observations of clusters of galaxies, strong gravity environments from observations of black hole systems, and cosmology through observations of the velocity structure in the intercluster medium. As a general-purpose observatory spectrometer, the SXS can be used for a wide variety of observations and investigations, from solar-system studies (charge-exchange processes), stellar atmospheres, binary systems (containing white dwarfs, neutron stars, and black holes), supernova remnants in our galaxy, to galaxies and clusters of galaxies out to a redshift of up to ~ 2 using exposures of 10^6 sec.

These objectives are achievable due to the extremely high spectral resolution, ΔE, of the SXS that is nearly constant with energy E, and the large bandwidth and non-dispersive characteristic of the sensor, an x-ray microcalorimeter array. With a resolving power, E/ΔE, that increases with energy, the energies of key spectral features can be measured precisely, particularly the He- and H-like iron complexes at 6.7 and 7.0 keV, respectively, that offer several powerful diagnostics. Such a capability allows the measurement of energies to a precision of 1 eV at 6000 eV, thereby enabling velocities to be measured to ~ 100 km/sec absolute, and velocity broadening of spectral features to ~ 10 km/sec.

The SXS uses an x-ray microcalorimeter array operating at 50 mK to obtain high spectral resolution (~ 5 eV FWHM throughout most of the 0.3–12 keV band) for both point and diffuse sources[2]. Combined with a low-temperature anticoincidence detector, it also has very low residual X-ray background, permitting the detection of weak spectral features with a residual background of only ~ 1 count/day/10eV over the full array. High sensitivity is obtained from the high detector quantum efficiency, highly transparent non-x-ray blocking filters, and a moderately high collecting area x-ray mirror (~ 320 cm^2 overall at 6 keV).

Although very simple in conceptual operation, the realization of a microcalorimeter spectrometer gives rise to a chain of complex requirements for a space-qualified instrument. These include a long-life, space-qualified dewar system capable of reaching 50 mK for many years, careful design of the array housing to prevent longer wavelength radiation from reaching the array (which essentially also operates as a highly sensitivity bolometer), an anticoincidence detector for identifying cosmic ray events, a low noise amplifier, and a complex pulse detection and analysis system for processing the x-ray events.

The dewar system that was adopted was designed to have redundancy so it could operate both with and without stored liquid helium (LHe). This required a series of mechanical coolers to provide cooling power at various stages of the dewar. Mechanical coolers by their nature produce vibrations, and these had to be decoupled from the detector stage in order to prevent vibration of sensitive

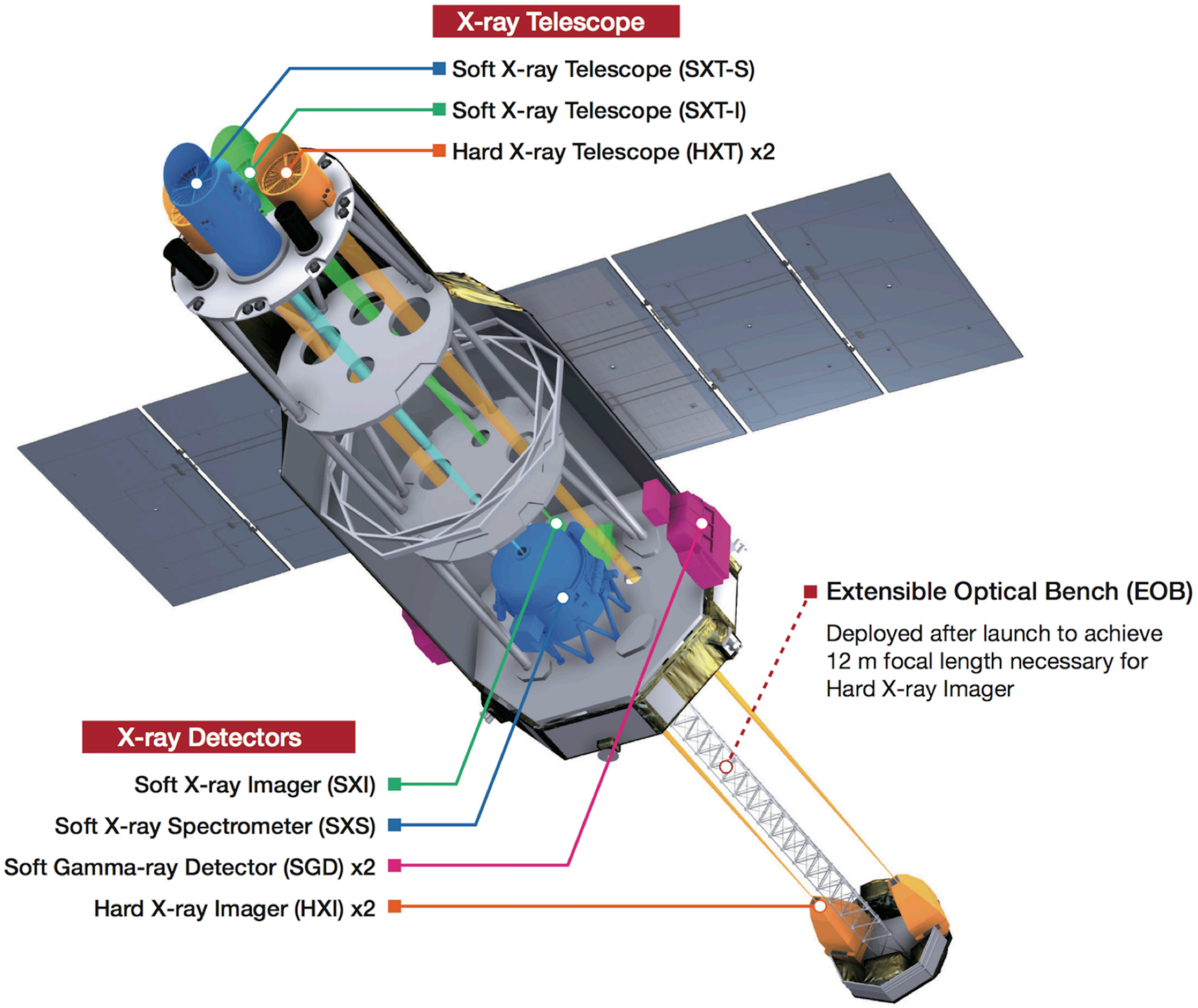

Fig. 1 Schematic view of the Hitomi X-Ray Observatory[1]. The overall length of the 2700 kg observatory is 14 m. All of the x-ray mirrors are mounted on a fixed optical bench, but the Hard X-Ray Imager (HXI) is mounted on a deployable boom that extends 6 meters for a total focal length of 12 m. The mirror SXT-S focuses x-rays onto the SXS and has a 5.6 m focal length.

electrical wiring (microphonics), and vibrational heating.

The SXS was developed jointly by the NASA/Goddard Space Flight Center and JAXA's Institute of Space and Astronautical Science. The US contribution was selected as a NASA mission-of-opportunity Explorer proposal in 2008. The responsibilities for the instrument were based on technology readiness and expertise, and evolved during the early stages of the collaboration as the instrument requirements were stabilized and the design optimized. As an example, initially it was planned that a 2K Joule-Thomson cryocooler stage would be available. This would permit both cryogen and cryogen-free operation for redundancy and maximum instrument lifetime. However, the cooler was not deemed ready to be baselined early enough, and it was thus decided to add an additional adiabatic demagnetization refrigeration stage to enable the required cooling options.

The SXS complements the operational grating spectrometers on *Chandra* and *XMM-Newton* in two important ways. For E > 2 keV, the SXS is both more sensitive and has higher spectral resolution, especially in the Fe K band where SXS has 10 times the collecting area and energy resolution. The SXS uniquely performs high-resolution spectroscopy of extended sources due to its

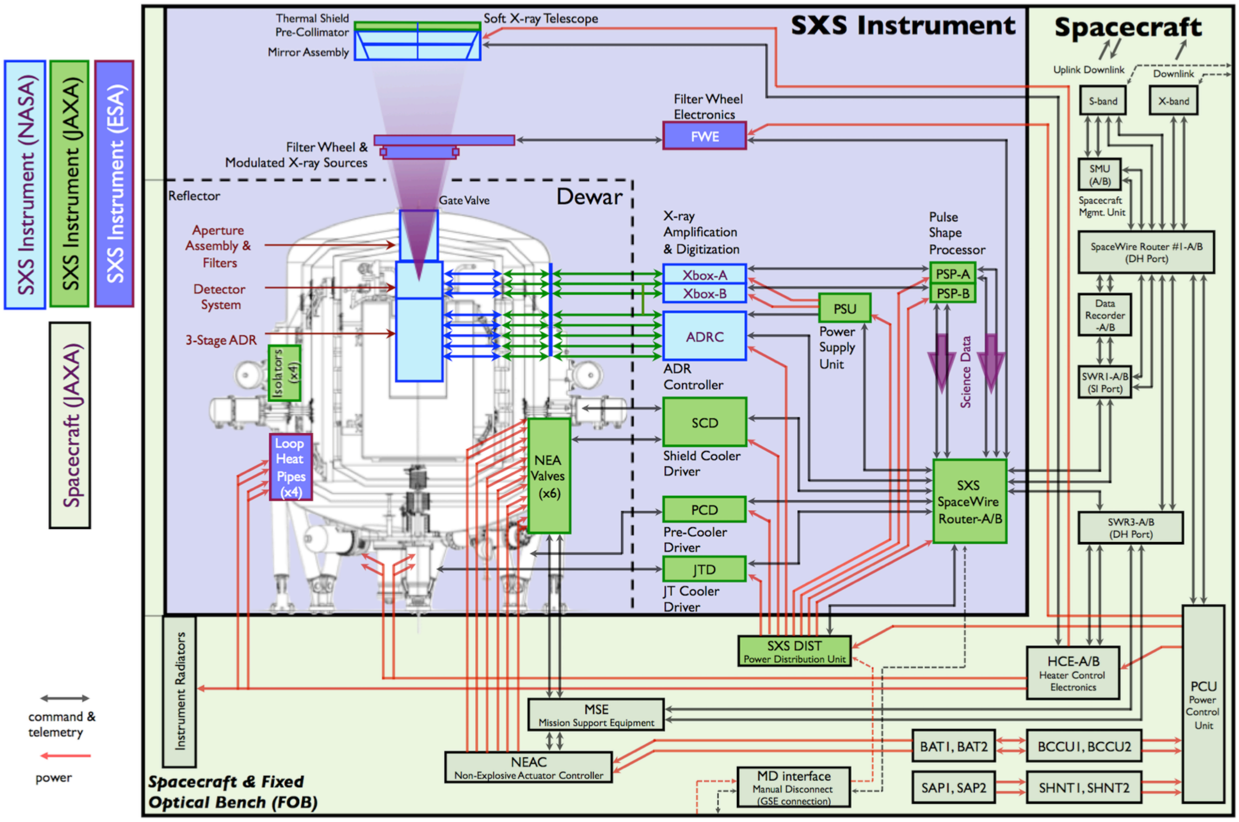

Fig. 2 Block diagram of the SXS instrument showing components, responsible agency, and interfaces.

non-dispersive operating principle. The SXS makes possible high-resolution spectroscopy of sources inaccessible to currently available grating instruments.

1.1 SXS instrument overview

The SXS has been described previously by Mitsuda et al.[3] The present paper serves as an update following completion of the instrument, its integration onto the satellite, and launch in February 2016. A block diagram of the instrument is shown in Fig. 2. X-rays enter the instrument from the top and are focused by the 5.6 m focal length soft x-ray telescope (SXT)[4]. The point-spread function of the SXT has a half-power diameter of 1.2 arcmin, which is an appropriate match to the comparatively large pixels of the array. Between the SXT and the dewar, there is a Filter Wheel (FW) and Modulated X-Ray Source (MXS) assembly.[5] The FW has six positions, including two OPEN position, two filters to attenuate the flux from especially bright sources (10's of counts/sec/pixel), one to provide a contamination barrier if needed, and a position with ^{55}Fe sources on a cross for in-flight calibration while simultaneously observing celestial sources. The MXS has four fluorescent x-ray sources. At the entrance to the dewar, there are five filters in series that prevent non-x-ray light from reaching the array. The five filters are attached at stages of the dewar dictated by overall optimal thermal design. The outer most three filters have integral heaters to remove adsorbed contamination if it is detected through x-ray measurements. The dewar main shell filter heater is operated continuously at approximately 300K to minimize accumulation of contaminants from the interior of the spacecraft.

At the focal point of the mirror is the x-ray calorimeter array, backed by an anticoincidence detector (antico) < 1 mm behind the array[6]. These are housed within a modular detector assembly that contains bias voltage dividers and JFETs as part of the first stage of readout electronics. There are also four thermal straps attached to the detector housing for connection to the cooling system, which is a series of three adiabatic demagnetization refrigerators (ADR)[7]. Stage 1 provides the 50 mK heat sink for the detector system. Stage 2 is cooled to 0.5K and serves as a heat sink for the Stage 1 ADR. The Stage 3 ADR is normally not in use but is activated when the He tank is empty. This capability allows the SXS to run in cryogen-free mode, which provides redundancy and can also be used to extend the life of the SXS after the liquid helium is exhausted (nominally after 3 years). The dewar has four concentric shields within the main shell cooled by various mechanical coolers and the venting He vapor. The three sets of mechanical coolers have dedicated cooler drive electronics.

The ADR Controller (ADRC) controls the three ADR stages, reads out thermometers, and provides heater power to the three outermost blocking filters. The Xbox provides the bias to the array and anticoincidence detector, amplifies the detector signals, and digitizes them for processing by the Pulse Shape Processor (PSP). The PSP performs a detection algorithm on all channels and then uses digital optimal filters to determine the pulse heights[8]. The ADRC is powered directly by the spacecraft power system while the Xbox receives power for analog and digital circuits from a Power Supply Unit (PSU). The Xbox is commanded via the PSP while the ADRC is commanded directly. Communication and data flow are handled by the SpaceWire system developed for the *Hitomi* mission.

In the following sections, we describe the elements of the instrument in further detail, and provide up-to-date references on the design and performance.

1.2 Microcalorimeter array

There are many x-ray microcalorimeter applications in use today. Arrays with superconducting transition edge sensor (TES) thermometers are more prevalent currently due to the prospects for fielding very large arrays through the use of multiplexed SQUID readout[9]. The SXS array is based on ion-implanted Si thermistors with HgTe absorbers developed in the 1990's[10]. This has been a good technology choice as it is extremely robust with respect to its operating requirements and has performed well in the space-instrument environment.

The array design is shown very schematically in Fig. 3. The fabrication starts with a silicon-on-insulator wafer that has a 380 μm backing wafer (dark gray) and a Si device layer that is 1.5 μm thick. The two Si layers are separated by a 0.2 μm insulating oxide layer. Photolithographic processes are used to delineate a 300 μm x 300 μm thermometer in the device layer for each pixel, with four right-angle beams attached to the thicker surrounding frame that flare out at the ends to

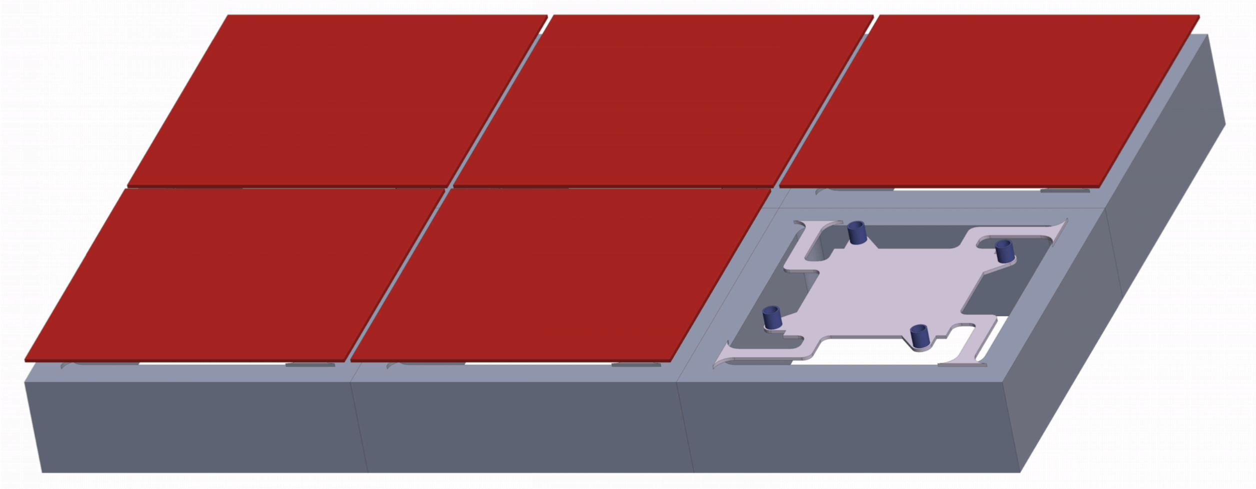

Fig. 3 Schematic representation of the microcalorimeter array, showing 6 of the 36 pixels. The light gray area is ion-implanted Si to form the thermistor. The thermistor area is suspended by the four right-angle beams connected to the Si frame (dark gray). The four blue posts are made from a polymer that allows the HgTe absorbers (dark red) to be attached in a controlled manner using epoxy. The absorbers are 819 μm on a side, and the pixel-pixel pitch is 832 μm. These give a filling factor for the array of 97%. The absorbers are about 10 μm thick, and absorb > 98% of incident photons at 6 keV.

reduce stresses. These beams form the weak thermal link between the thermometer area and the frame required for calorimeter operation. The thermometer area is ion-implanted with P compensated with B to form a hopping-conduction thermistor with a high temperature coefficient (R ~ T^{-6} at operating temperature).

The next major components are the x-ray absorbers attached to each pixel (dark red in Fig. 3). The absorbers are attached with epoxy to small polymer tubes that are located on four positions of the implanted thermometer area. These are necessary for well-controlled attachment of the absorbers and to produce high uniformity of the thermal conductance between the absorber and the Si thermistor body. This control is necessary to obtain a high degree of energy-resolution uniformity across the array. The requirements for the absorber material are low heat capacity below 100 mK, rapid (< 100 μsec) and reproducible thermalization of x-rays, and high absorption coefficient for x-rays up to 12 keV. To subtend the required 3 × 3 arcmin field of view in a 6 × 6 array given the 5.6 m focal length of the optical system, a pixel pitch of 832 μm is required. The absorber material used is the semi-metal HgTe, known for its excellent x-ray thermalization properties, theoretically low heat capacity, and high x-ray absorption. The actual absorbers measure 819 × 819 × 10.5 μm. This provides pixels that are 30 arcsec on the sky with an overall field of view of 3 arcmin. The geometric filling factor of the array is 97%. The energy resolution of the array is ~ 4 eV measured at 6 keV at the component level.

1.3 Detector Assembly

The detector assembly (DA) houses the calorimeter array, antico, and front-end electronics[11,12]. The basic requirements on the DA are to provide a modular assembly that thermally isolates and encloses the microcalorimeter array so it can be temperature-controlled at 50 mK to better than ~ 2.5 μK rms.

In addition, the DA must limit the amount of non-X-ray power reaching each pixel to less than ~ 10^{-13} W/pixel, which would be enough to diminish their sensitivity.

The mechanical design must provide a high degree of strength to withstand launch vibration forces (which are mainly below 100 Hz). To achieve this, the mechanical resonances within the DA are designed to be all above 300 Hz. The basic approach is to mechanically support the detector housing and the JFET assemblies with tensioned Kevlar® because of its excellent strength and low thermal conductance, and to use tensioned electrical wires to obtain high resonant frequencies. The connection of the detector housing to the ADR is made with four gold plated copper straps that are annealed to provide high thermal conductance.

Microcalorimeters with thermometers based on doped semiconductors typically have electrical impedances > 10's MΩ. With such high impedance, the effects of coupling capacitance to the dewar over long wiring runs can lead to high susceptibility to microphonics. To avoid this problem, a simple JFET source-follower circuit is employed to transition from the high impedance of the detector to the much lower output impedance of a JFET, which is of the order of 1 kΩ. The basic circuit is straightforward to implement[11,12]. One complication that arises is that the low noise JFETs adopted must operate at a temperature of about ~ 130 K. This requires careful thermal staging of the JFETs in order to minimize their heat load on the He cryostat and also prevent their thermal emission and conducted heat from reaching the detector stage.

Because the detector resistance has a negative temperature coefficient, the detector is current-biased in order to achieve negative electrothermal feedback (i.e., $dP/dT < 0$, where $P = I^2R$). This is done (to a good approximation) with ~134 MΩ load resistors in series with the detector, which operates at about 30 MΩ under the nominal bias. A voltage divider is employed to attenuate input noise on the externally applied bias of 1.6 V by a factor of 121. For redundancy, the bias circuit is actually divided up into four groups of 9 channels each. The 1 MΩ resistors of the divider are heat sunk at 28 K (the inner vapor-cooled shield) in order to avoid dissipating Ohmic power to the He tank (about 8 μW total). The other resistors of the divider dissipate < 1 μW to the He tank. The output return lines have 2 kΩ resistors on them (one for each channel) in order to approximately balance the output impedance of the JFETs for the differential preamplifier of the analog electronics outside the dewar.

The 50 mK detector enclosure has two gold-plated alumina feed-through blocks that contain the 134 MΩ load resistors (at 50 mK) that are epoxied in place and coated with silver-filled epoxy to prevent light leaks. The lid to the enclosure fits with a tongue-and-groove arrangement for a light seal and has a radioactive source (^{55}Fe) on top that is collimated to illuminate a special pixel on the frame of the array that is identical to the array pixels, but outside the field of view. This is useful for continuous gain monitoring of the overall calorimeter gain and also for ground testing when it is not possible to illuminate the array externally.

1.4 Adiabatic Demagnetization Refrigerator (ADR)

The ADR is used to cool the detector array to 50 mK[7]. This cooling technique was adopted because of its simplicity and suitability for spaceflight. No moving parts or gravity are required for operation. Briefly, the ADR works by using a system of magnetic spins (a paramagnetic salt) with interaction energy at 1 K much lower than kT (where k is Boltzmann's constant) to exchange the entropy of an ordered system of spins at higher temperature for that of a relaxed system at lower temperature. The spins are aligned using an external magnetic field (~ 2 Tesla) and the heat of magnetization is conducted away to the He bath through a heat switch. This lowers the entropy of the spin system isothermally. A heat switch is then opened and the magnetic field is reduced, causing the spins to demagnetize adiabatically, and the system to cool. In practice, the magnetic field is ramped down to a finite value such that the temperature of the paramagnetic salt is 50 mK, and the remainder of the cooling power is used to regulate the temperature at this value for an extended period of time.

The SXS contains three separate ADRs. Stage 1 provides 50 mK cooling for the detector system, Stage 2 provide 0.5 K cooling and is used as the heat sink for Stage 1. Stage 3 is used to cool the CSI interface (He tank) to ~ 1.5K when the tank is empty, thereby enabling cryogen-free operation. The hold time at 50 mK is determined by the parasitic heat loads on the ADR stages, the temperature of the LHe cryostat, and optimizing the cycling profile (e.g., the dI/dt of the magnets and operation and phasing of the heat switch ON/OFF times). During ground testing, the hold time was typically 42 hours. In orbit, as the LHe cryostat cooled below 1.2K and the hold time reached 48 hours, resulting in an overall 50 mK operating efficiency of 98%.

Separate ground testing of the cryogen-free mode was carried out[13]. Without the high heat capacity of the superfluid LHe, the system is much more sensitive to rapid temperate changes, in particular the 4.5 K Joule-Thomson cooling stage. This required a different optimization of the ADR cycles in order to keep the helium tank temperature (which directly couples to the DA) stable to within 1 mK rms at a temperature less than 1.8 K. In this case, Stage 3 is continuously operated, but the Stage 1 and 2 cycles are operated with a recycle time of 2.5 hours and a hold time of 14.5 hours at 50 mK within the required stability of 2.5 μK rms. This gives an operational efficiency of 84%. This is quite acceptable since the overall observatory efficiency is determined by operations in low earth orbit (~ 40%).

Fig. 4 The integrated SXS detector and ADR assembly being installed into the flight dewar in March 2014 at Sumitomo Heavy Industries, Japan.

1.5 Calorimeter Spectrometer Insert (CSI)

To facilitate a simple interface between the detector system, ADRs, and the dewar, the DA and ADRs were integrated into a subsystem in the US, designated the Calorimeter Spectrometer Insert (CSI), and then delivered to JAXA where it was installed as a unit into the dewar system (Fig. 4). An interface plate was produced by the dewar manufacturer (Sumitomo Heavy Industries), and then shipped to the US where the DA and ADRs were attached. The CSI was tested in a specially designed test dewar at Goddard and also vibrated at 77K in a custom made vibratable dewar for flight qualification.

The other major component of this system is the high temperature superconducting leads, or HTS leads[14]. These are a critical component of the instrument for providing the required high electrical current (up to 2A) to the ADR solenoid magnets with minimal thermal conductance. The HTS conductor is primarily a YBCO high-temperature superconductor on a low-conductance substrate (Hastelloy) in the form of a ribbon that has an overall dimension of 1 mm wide × a few μm thick. The ribbon is coated with a thin layer of sputtered Ag to protect it from water vapor, CO_2, and loss of oxygen. The leads were divided into two groups: one pair for Stages 1 and 2, and one for Stage 3. The leads were secured to custom-made T300 composite support structures (Fig. 5). The HTS leads are anchored at the inner vapor-cooled shield on the warm end (nominally 28 K), and on the other end to normal superconducting leads made from Cu-clad NbTi that are part of the ADR solenoid magnets.

1.6 Dewar

The design of the dewar system for the SXS is based on stored liquid helium guarded with mechanical cryocoolers[15]. The key design requirement of the dewar is redundancy with respect to stored cryogen loss and mechanical cooler failure. Starting from the outside, there is a vacuum main shell that cools to ~ 260 K with the dewar is in orbit, mounted on the anti-Sun side of the spacecraft. Within the main shell, there are three nested vapor-cooled shields, with thermal connections to the He tank vent line. These are the outer, middle, and inner vapor cooled shields (OVCS, MVCS, and IVCS). The typical operating temperatures are 120K, 80K, and 28K, respectively. The first and second stages of a pair of Stirling coolers are connected to the OVCS and IVCS. These coolers are redundant in the sense that they are nominally operated at half power, but either can be operated at full power in the event that the other is not operational.

Inside the IVCS is the Joule-Thomson (JT) shield, cooled to 4.5 K with a ^{4}He JT cooler. This cooler has low- and high-pressure compressors and a separate pair of 2-stage Stirling coolers used for pre-cooling. In operation, the LHe is pumped by space vacuum to < 1.2K through a porous plug/superfluid film killer assembly[16].

During testing of the engineering model of the SXS, it was recognized that vibration from the Stirling cooler compressors caused excessive vibration at the 50 mK stage, which created time-variable heating that blurred the energy resolution. After extensive testing and characterization, mechanical isolators were adopted that were highly successful[17]. With the isolators in place, the coolers have virtually no impact on detector performance.

1.7 Blocking Filters

The blocking filters are a fundamental component of the SXS[18]. The filters prevent radiation with wavelengths longer than x-rays from reaching the detector and have to be optimally staged within the dewar to minimize heat loads. The long wavelength radiation can potentially heat up the pixels or induce photon shot noise and the filters must be designed and staged within the dewar to prevent this. The filters also close out thermal shields of the dewar to minimize heat loads on the colder stages of the dewar (particularly the LHe). An important driving factor in the original design of the filters was the need to keep the potentially high-flux of He II Lyα geocoronal emission line (304 Å = 41 eV) from reaching the detector. Including the aluminized polyimide on the thermal shield of the SXT[4], the filter design actually has substantial margin for attenuating this emission. There are other stringent requirements on the longer wavelength UV, visible and IR rejection, but with the basic design of the SXS filters (five filters in series), these are easily met once the geocoronal emission is

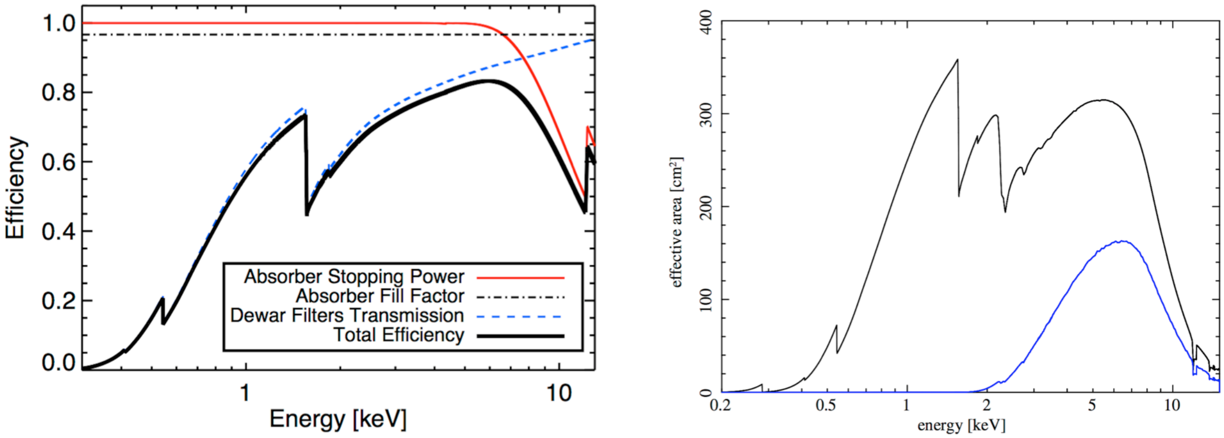

Fig. 6 (Left) The efficiencies of key components of the SXS that determine the net throughput. (Right) Effective area of overall SXS instrument with the SXT. The black curve is the nominal end-end effective area while the blue curve shows the area with the aperture door closed. The aperture door has a Be window with a thickness of ~ 260 μm and a stainless steel protection screen.

appropriately attenuated.

These requirements set the minimum total thickness of the filters, but there are other factors that had to be included as well. These were the need to survive numerous thermal cycles to very low temperatures, mechanical vibration, pressure gradients of a few torr, and be sufficiently non-permeable to water vapor at room temperature. Through years of testing, and feedback with the manufacturer of the filters, Luxel Corporation, we arrived at the filter parameters described in Ref. 18. The filters are aluminized polyimide and are highly reflective in the visible and IR. The UV attenuation is determined by both the aluminum and polyimide thicknesses. The outermost three filters are supported by custom-made Si meshes that have both fine and coarse mesh patterns to provide higher mechanical strength for these larger filters. The meshes also provide high thermal conductance across these filters for defrosting/decontamination by the heaters if necessary. The net detection efficiency of the array, including the transmission of the filters, absorption efficiency, and array fill factor are shown in Fig. 6 (Left).

The main shell and OVCS filters are mounted at opposite ends of a cylinder made from the composite gamma-alumina and lined with a thin, low thermal conductance sheet of the alloy Ti-3-3-3[18]. The cylinder is attached to the main shell of the dewar. The cylinder provides a vapor barrier from the multi-layer insulation that is in place between the dewar shields. The outermost layers are warm enough under normal operation that the continuous outgassing of air and water could potentially reach and be adsorbed onto the cold filters.

1.8 Instrument Electronics

There are four main categories of instrument electronics for the SXS. These are the Xbox, Pulse Shape Processor (PSP), ADR Controller (ADRC), and the cooler drive electronics. In addition, there is a separate power supply unit (PSU) to the Xbox. The PSP and ADRC interface to the spacecraft telemetry system via SpaceWire routers. There are three separate cooler drive electronics modules (Ref. 15 and references therein): the shield coolers (SCD), the pre-coolers (PCD), and the JT cooler (JTD).

1.8.1 Xbox

The Xbox, located outside of the SXS instrument dewar, amplifies and digitizes the signals from each detector channel (Fig 7). It also provides the bias voltages for the calorimeter and anticoincidence (antico) detector, and the supply voltages for the cold (130K) JFET boards located within the DA. The outputs of the JFETs provide the low-level analog signals to the Xbox.

The general design of the Xbox is to divide the functions into two independent sides that are

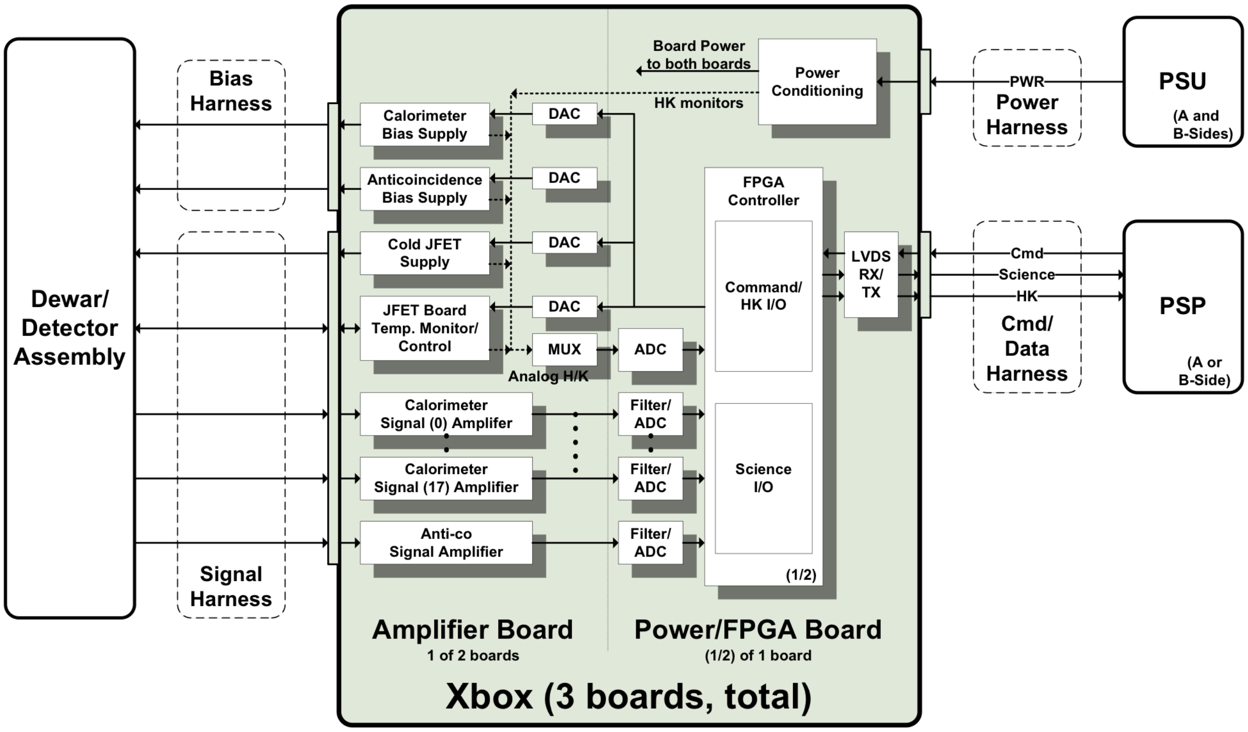

Fig. 7 Functional block diagram of Xbox, the calorimeter amplifier, digitizer, and control unit.

nominally operational, so redundancy is achieved by segmentation. As shown in Fig. 7, there are two amplifier boards, each providing 19 channels (18 calorimeter + 1 antico). The Xbox is powered by the PSU, providing ±13.50V, ±5.60V, and +5.00VD separately for the A and B sides of the Xbox. This regulated power is filtered and post-regulated within the Xbox to provide the necessary supply voltages throughout the Xbox.

The resulting signal voltages are amplified, digitized, and packetized for each sampling interval, and transmitted to the Pulse Shape Processor (PSP) communication interface. The default sampling rate is 12.5 kHz (80 μsec samples), and an optional sampling rate of 15.625 kHz (64 μsec samples) can also be selected. The sample size is 14 bits in both cases. The amplifier gain is 2500 for both the calorimeter and anticoincidence signals, and the input-referred amplifier noise (calorimeter and anti-coincidence amplifiers) from 30Hz to 2.0kHz is < 5.0nV/√Hz.

The Xbox is commanded via the PSP subsystem to initialize parameters and control its operation. In response to each command packet received from the PSP, the Xbox generates command response packets in the form of housekeeping data consisting primarily of board status information. These command response packets are transmitted through the PSP communication interface.

1.8.2 PSP

The main function of the PSP is to take the digitized stream from each calorimeter channel and the two antico channels, trigger on the events, and then analyze the events for pulse height and arrival time[8]. The PSP implements an optimal pulse height determination algorithm that maximizes the signal-to-noise estimate of each pulse height with respect to the actual broad-band noise of each channel as determined by accumulating noise spectra when x-rays are not present. This allows for optimal performance under actual flight conditions. Based on the implementation described in Ref. 19, a series of coefficients are generated and then multiplied and summed for each pulse. The optimum phase between the template and each pulse is determined and the pulse height is derived for that phase. The coefficients can be computed on board or on the ground on the basis of data previously recorded, and then uploaded. As the count rate from a source increases, the resulting pulse pile-up will eventually compromise the pulse height determination. To deal with this, the PSP processes events differently according to their relation in time to other events. There are three "grades" of events, high, mid, and low, depending on the relative inter-pulse arrival times[20]. This results in a larger fraction of events with high resolution. These grades are recorded with each event and the user can specify which are to be used for analysis. The PSP also computes pulse rise times, which are used to screen abnormal events, antico pulse heights, arrival times, commanding and clock synchronization with the Xbox, transmitting all pulse event and housekeeping data to the spacecraft telemetry system.

1.8.3 ADRC

The Adiabatic Demagnetization Refrigerator Controller (ADRC) is used for temperature monitoring, cycling, and temperature control of the 3 ADR stages, and temperature control of the three outermost blocking filters. The ADRC is powered directly by Astro-H bus power and internally generates the low-level voltages and low (nano-amp) thermometer excitation currents, and communicates with the spacecraft via the SpaceWire interface.

Referring to the functional block diagram in Fig. 8, the temperature monitoring and control for each ADR stage is carried out by three separate ADR Monitor and Control (AMC) boards, referred to as CAMC, WAMC, and HAMC ("Cold", "Warm", and "Hot") for stages 1, 2, and 3, respectively.

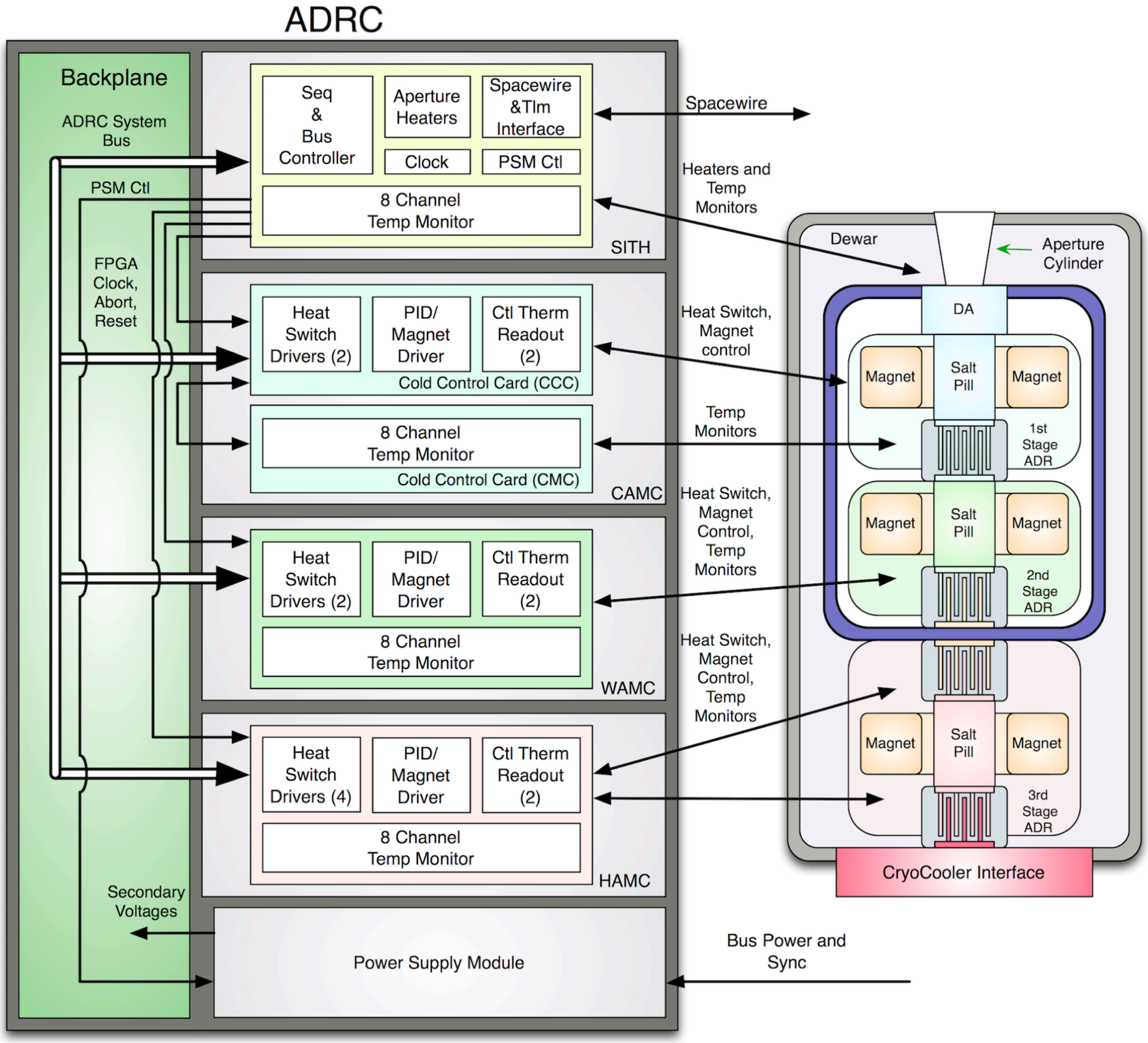

Fig. 8 Functional block diagram of the ADR Controller (ADRC) and its interfaces to the internal dewar components.

The Temperature Monitor (TM) circuits on each card measure the resistance of up to 8 thermometers. Each channel also has a dedicated precision resistor (100 kΩ) that is switched in for calibration or to remove that stimulus from the thermometer. The measurements are done in parallel by using a modified auto-correlation technique. Each of the 8 thermometers is independently stimulated by a dedicated current source operating at a unique, fixed frequency. The stimulus is digitally synthesized via an EEPROM and 16 bit DAC. The EEPROM contains 4096, 16 bit samples for both a sine and cosine of each frequency taken over exactly 1 second. The voltage returns from each sensor are independently amplified and summed together. The sum is then sampled via a 16 bit ADC at 65536 samples/sec. A modified auto-correlation algorithm is then used to process the samples to obtain the individual temperature values. After a 1 sec measurement interval, the accumulated sum for each frequency is divided by a calibration factor for a given channel, producing a resistance measurement.

The control thermometer readout circuit is a single channel version of the temperature monitor circuit. The stimulus frequency is 18 Hz. Relays are used to select the calibration resistor or one of two thermometers. The return is amplified, filtered and sampled at 65536 Hz. 16 samples are grouped, summed and processed by a single frequency auto-correlation algorithm. The result is accumulated for nominally 18 cycles. The accumulated sum is then divided by a calibration factor, producing a resistance measurement. The AMC cards have the capability of converting the measured thermometer resistance to temperature. The conversions are performed automatically by the AMC FPGA for all Control and Monitor channels once per second. The results of the conversions are stored in registers accessible via backplane reads.

1.9 Filter Wheel/X-Ray Calibration Sources

For in-flight calibration and attenuating the x-ray flux from some galactic x-rays sources, a Filter Wheel/Modulated X-Ray Source (FW/MXS) assembly is mounted about ~ 90 cm above the dewar on a lower baffle of the spacecraft fixed optical bench[5]. The FW has six positions, listed in Table 1.

Table 1 Filter Wheel Positions

Open (2 positions, 180° apart)	
Neutral density	Hole pattern – 24.5% throughput. Mo (250 μm thick)
Low energy attenuation	Be ~ 26 μm thick
Contamination	Polyimide (211 nm) + mesh (86.5% open)
Calibration	^{55}Fe sources mounted on a cross to allow simultaneous illumination with celestial source.

The MXS consists of four x-ray sources based on light-sensitive photo-cathodes to generate electrons that are accelerated to 11.3 kV with high voltage towards a target. The light produced by UV LEDs can be pulsed very rapidly, which provides for simultaneous x-ray calibration data with a known duty life fraction. This allows for essentially continuous energy gain scale determination while observing without contaminating the astronomical data.

The four MXS units are grouped into two identical pairs for redundancy. One set has the target material deposited on the Be window that seals the source to create a "direct" source of higher energy lines (Cr: 5.41, 5.95 keV, and Cu: 8.05 and 8.90 keV) while the other pair have a fluorescent target mounted at 45° outside of the Be window with Al (1.49 keV) and Mg (1.25 keV) to create lower energy lines. The initial planned pulse period for the direct source was 5 msec with a duty cycle is 8%, and 12.5 msec and 20% duty cycle for the weaker, indirect source. Although successfully tested during pre-launch thermal-vacuum testing, the operation of the LEDs was not carried out in orbit due to the loss of the spacecraft on March 26, 2016.

1.10 Soft X-Ray Telescope

X-rays are focused onto the microcalorimeter array by the soft x-ray telescope. This is a two-reflection, conical approximation to a Wolter Type I x-ray mirror[4]. The focal length is 5.6 m. The mirror has 203 concentric shells grouped into four quadrants (each of which has primary and secondary reflectors) for a total of 1624 reflectors. The reflecting surface is gold. The mirror has a diameter of 45 cm and a mass of 43 kg. The overall point-spread function is 1.2 arcmin (half-power diameter)[21]. Fig. 6 (Right) shows a plot of the end-end effective area of the instrument based on synthesizing all of the SXS and SXT calibration data[22]. The black curve is the expected, nominal effective area with the dewar aperture door open, while the blue curve is the area with the dewar aperture door closed. The door has a Be window (~ 260 μm) and a stainless steel screen (71% open).

2 Instrument Performance

Following completion of the SXS in late 2014, there was extensive ground testing prior to spacecraft integration and launch.

2.1 Ground tests and Calibration

The SXS was calibrated at the component level as flight components became ready, and then tested extensively at the instrument level from late 2014 through launch in February 2016 (Ref. 22). The test campaign included comprehensive functional performance tests before and after environmental tests at the subsystem level, and then at the spacecraft level, including spacecraft-level thermal vacuum test. Testing was carried out in both cryogen mode and then over a more limited time in cryogen-free mode. Overall, the tests were extremely successful in verifying the performance of the instrument and identifying potential problems. The issue of vibration from the mechanical coolers was discovered during tests with the engineering model, as addressed in Section 1.6 above. During early tests of the flight dewar, new tests were conducted without cooler isolation to see if the disturbances induced by the coolers were still present, and at the same level. It was found that the level of disturbance was much lower, likely due to the higher thermal conductance between the detector housing and the ADR (which resulted in lower temperature excursions), but the disturbances were still present. It was decided that there was not sufficient margin against meeting the 7 eV energy resolution requirements, and that the isolator should be adopted for flight[17].

Another problem that was discovered in ground testing was disturbance from the magnetic torquer (MTQ) solenoids used for spacecraft angular momentum management. Noise in the data corresponding to the pulse width modulating power switching frequency (127 Hz) was picked up by the detector system. This noise was studied in detail and found to vary with pulse width duty cycle. Also, the rotation speed of one of the reaction wheels (unit 3) was picked up by the detector system, presumably due to vibration. For both of these interference effects, tests were carried out to simulate real orbital operations, where the MTQ duty cycle and reaction wheel speeds vary continuously, and it was found that the overall disturbance was small and resulted in only a small increase to the energy resolution (~0.2 eV), thus it was deemed acceptable to proceed toward launch.

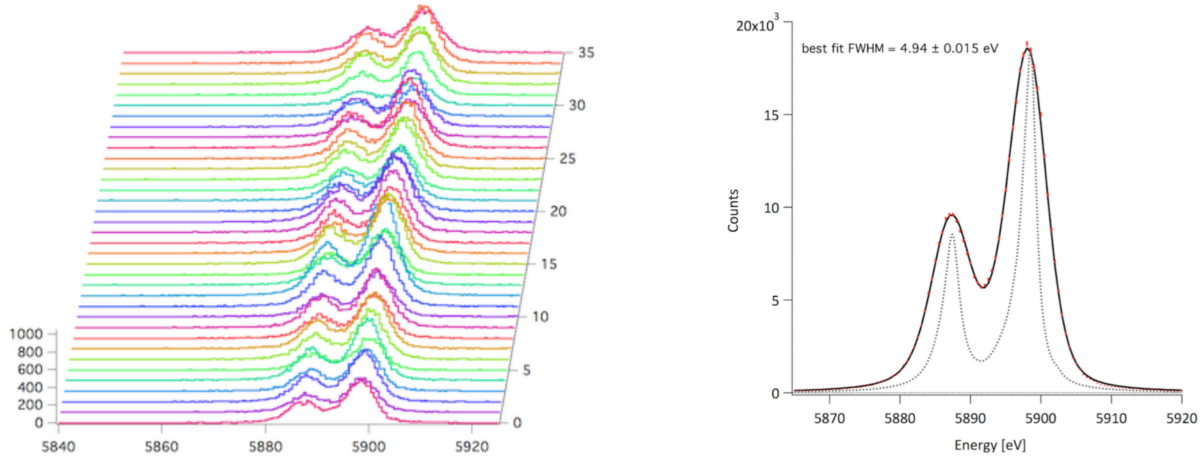

Fig. 9 (Left) The response of the array to the ^{55}Fe calibration sources mounted on the Filter Wheel. The data were taken in orbit on 19 March 2016. (Right) Stacked spectra from the ^{55}Fe source, demonstrating an energy resolution of 4.9 eV.

2.2 *In-flight*

The Hitomi satellite was launched on 17 February 2016 at 17:45 JST from the Tanegashima Space Center. The launch was flawless and the spacecraft reached its intended orbit of 575 km circular to within 1 km. Details of the in-flight operation of the SXS are described in Ref. 23. Briefly, on Day 5 of the mission the SXS was successfully cooled to 50 mK. The instrument demonstrated nominal performance, and excellent consistency with pre-flight operations[24]. The spacecraft was then slewed to the Perseus Cluster of Galaxies on Day 7 (24 February 2016). This target was chosen because of its large angular size compared with the 3 arcmin field of view of the SXS and its high x-ray surface brightness. Spectra immediately revealed that the cluster is rich with line features, as expected, but that the velocity broadening of the lines is relatively small, less than 200 km/sec. This is on the spatial scale of the 30 arcsec pixels (~ 10 kpcs at Perseus) and 1.2 arcmin HPD. The ^{55}Fe position on the FW was selected 13 days after this observation and used to calibrate the energy scale and extrapolate back to the time of the Perseus observation[25]. The Perseus results have been published[26] and demonstrate the power of x-ray microcalorimeters for new astrophysics.

The dewar system required careful attention prior to launch to maintain a high volume of superfluid He. Spacecraft and rocket operations required frequent periods where the cryocoolers were turned off. Nonetheless, a fill volume of 97% superfluid was achieved prior to launch. Measurement of the flow rate from the temperature gradient across the porous plug indicated nominal heat load to the He tank. Further, the transient increase of the He bath from each ADR cycle was used as a mass gauge of the He volume. These data were all consistent with a lifetime of > 4 years[7,15].

Table 2 SXS Energy Resolution Budget

Nominal bias, at 6 keV				
	eV FWHM			**eV FWHM**
Base Ideal model	**2.7**			**2.9**
	Allocation (eV)	**Allocation in in units measured**	**Estimated in-flight actual in units measured**	**Estimated actual (in eV)**
Detector system budget				
excess broadening	3.5	3.5 eV	< 2.5 eV	2.5
sub-mm photon noise	2	140 fW from 1.8K	< 70 fW from 1.13K	1.1
JFET noise	2	white noise: 9 nV/√Hz	6 nV/√Hz	1.6
		1/f noise: 16 nV/√Hz at 10 Hz	4 nV/√Hz at 10 Hz	
cosmic-ray heating	3	XRS sensitivity	SXS sensitivity	1.6
microphonic tone	1.2	loss of single low-freq bin	none	0.0
Other subsystems				
ADRC temperature control	1.2	2.5 µK RMS	2 µK RMS including cosmic ray interaction in thermometers (0.5 µK RMS on ground)	1.0
Xbox bias noise	0.2	7.3 nV/√Hz	0.5 nV/√Hz	0.2
Xbox bias stability	1.8	0.015% RMS	Temp coeff < 100 ppm/K and typical rate of change 0.12 K/600s	0.3
Xbox amplifier noise	1	white noise: 5 nV/√Hz	2 nV/√Hz	0.6
		1/f noise: 5 nV/√Hz at 10 Hz	2 nV/√Hz at 10 Hz	
XBox gain stability	2	0.012% RMS	Temp coeff < 100 ppm/K and typical rate of change 0.12 K/600s	0.1
PSP computational error	0.5	0.5 eV	0.5 eV	0.5
ADRC ~1K interface stability	1	1 mK RMS	0.2 mK RMS	0.1
Unallocated Margin	0.7			0.0
interference from AOCS			1.6 eV	1.6
RSS of base and noise	**7.0**			**5.0**

As a way to summarize the performance of the SXS in orbit, we show in Table 2 the energy resolution budget allocations used to guide the design of the instrument during its development and the actual contributions to the resolution in the finished, operating instrument in orbit. It shows the factors that contribute to broadening the energy resolution over the intrinsic, base resolution of the array in the relevant units of the contributor (e.g., temperature fluctuations in K, etc.) and then the resultant contribution in eV. The overall resolution from all of these terms is the root-mean-square of all of the terms, and is shown at the bottom. The base energy resolution comes from a model of the calorimeter pixels based on lab measurements (I-V curves, pulse shapes)[6]. Note that the detector model changed somewhat between the design guide and the final assessment, which is why the base resolutions and relationships between noise values and contributions in eV are not the same in the two columns. The original model was based on the thermistors of the Suzaku XRS calorimeter[10], but the SXS thermistors ended up being slightly less sensitive. Note also that a different basis was used to express the original allocations and the in-orbit assessments for gain and bias stability. Some subsystems needed much less than their full allocations, allowing improved performance over that required despite the added noise from the attitude operations control system (AOCS). Note that the AOCS noise was not stationary; the number in the table is a representative number from ground tests at fixed settings. The effects of cosmic-ray heating for both XRS (the original allocation for SXS) and SXS were taken from the dependence of resolution on cosmic-ray rate; the values shown are for the average rate. The actual energy resolution is very close to the expectation (i.e., 4.9 eV vs. 5.0 eV).

Finally, in Fig. 10 we show the residual x-ray background of the SXS obtained from 366 ksec of Earth eclipse data. Using the antico to veto coincident cosmic-ray events on the array, event screening by rise time, and vetoing on pixel-to-pixel coincidence, we derive a residual x-ray

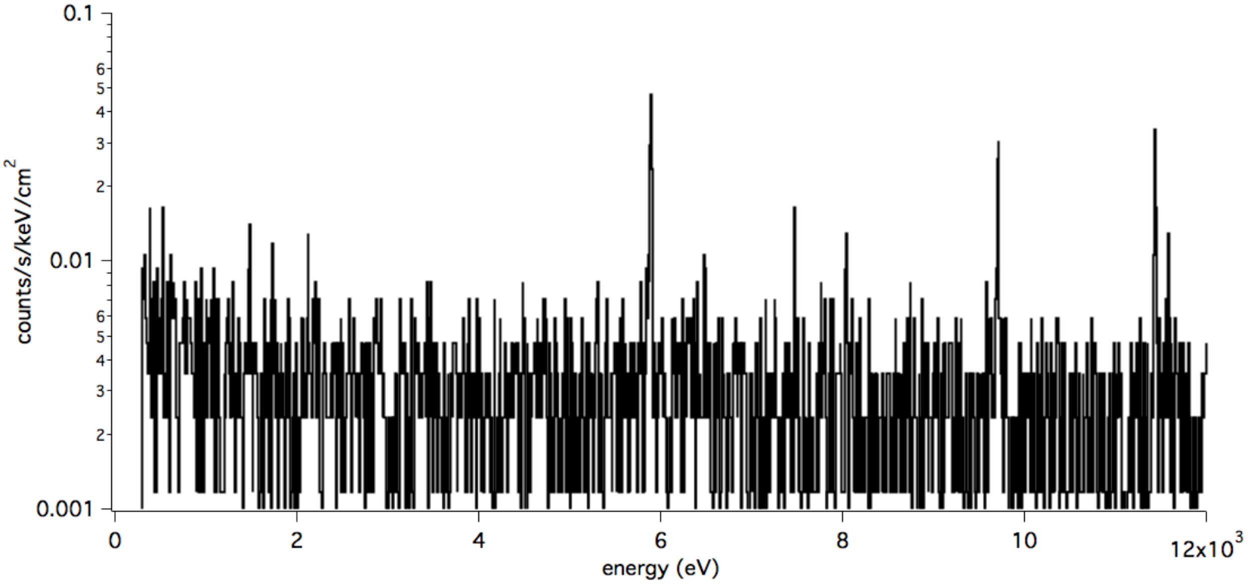

Fig 10 Residual x-ray background over the 35 pixels in the field of view of the soft x-ray telescope. The background was obtained after applying the anticoincidence and standard data screening criteria.

background of 3×10^{-3} cts/s/keV/cm^2 over 0.3-12 keV. A comprehensive report on the SXS background is presented elsewhere.[27]

This manuscript is based on the paper of the same title by Kelley et al., *Proc. SPIE* **9005**, 99050V-1 (2016).

Acknowledgements

The authors are extremely grateful to hundreds of people at the Goddard Space Flight Center, the University of Wisconsin, the Institute for Space and Astronautical Science and numerous other institutions in Japan for their tireless efforts in bringing the SXS to fruition. The Luxel Corporation has also contributed greatly to the design, manufacture, and reliability of the blocking filters, and the team acknowledges the extremely hard work and dedication of the dewar team at Sumitomo Heavy Industries in Niihama, Japan.

References

1. T. Takahashi, et al., “The Astro-H x-ray astronomy satellite,” *Proc. SPIE* **9905**, 99050U (2016).
2. S. H. Moseley, J. C. Mather, and D. McCammon, “Thermal Detectors As X-Ray Spectrometers,” *J. Appl. Phys.* **56**, 1257, (1984).
3. K. Mitsuda, et al. “Soft x-ray spectrometer (SXS): the high-resolution cryogenic spectrometer onboard Astro-H,” *Proc. SPIE* **9144**, 91442A (2014).
4. Y. Soong, et al., “Astro-H soft X-ray telescope (SXT),” *Proc. SPIE*, **9144**, 914428 (2014).
5. C. P. de Vries, et al., “Calibration sources for the soft x-ray spectrometer instrument on Astro-H,” *Proc. SPIE*, **8443**, 8443–53 (2012).
6. C. A. Kilbourne, et al., “The design, implementation, and performance of the Astro-H SXS calorimeter array and anti-coincidence detector,” *Proc. SPIE* **9905**, 99053L (2016).
7. P. J. Shirron, et al., “Design and on-orbit operation of the adiabatic demagnetization refrigerator on the ASTRO-H soft x-ray spectrometer instrument,” *Proc. SPIE* **9905**, 99053O (2016).
8. Y. Ishisaki, et al., “In-flight performance of pulse processing system of the Astro-H soft x-ray spectrometer.” *Proc. SPIE* **9905**, 99053T (2016).
9. K. D. Irwin, and G. C. Hilton, in “Cryogenic Particle Detection”, Topics Appl. Phys. **99**, 63-149, Ed. Chr. Enss, Springer-Verlag (2005).
10. C. K. Stahle, et al., “The next generation of silicon based x-ray microcalorimeters,” *Proc. SPIE* **4851**, 1394-1403 (2003).
11. F. S. Porter, et al., "The detector subsystem for the SXS instrument on the Astro-H observatory," *Proc. SPIE* **7732**, 77323J (2010).

12. M. P. Chiao, et al., “System design and implementation of the detector assembly of the Astro-H soft X-ray spectrometer,” *Proc. SPIE* **9905**, 99053M (2016).
13. G. A. Sneiderman, et al., “Cryogen-free operation of the soft x-ray spectrometer instrument,” *Proc. SPIE* **9905**, 99053N (2016).
14. E. R. Canavan, B. L. James, T. P. Hait, A. Oliver, and D. F. Sullivan, “The Astro-H high temperature superconductor lead assemblies,” *Cryogenics*, **64**, pp. 194-200 (2014).
15. R. Fujimoto, et al., “Performance of the helium dewar and cryocoolers of Astro-H SXS,” in *Proc. SPIE* **9905**, 99053S (2016).
16. Y. Ezoe, et al., “Porous plug phase separator and superfluid film flow suppression system for the soft-x-ray spectrometer onboard Astro-H,” *Proc. SPIE* **9905**, 99053P (2016).
17. Y. Takei, et al., “Vibration isolation system for cryocoolers of Soft X-ray Spectrometer (SXS) onboard Astro-H (Hitomi),” *Proc. SPIE* **9905**, 99050X (2016).
18. C. A. Kilbourne, et al., “The design, implementation, and performance of the Astro-H SXS aperture assembly and blocking filters,” *Proc. SPIE* **9905**, 99053Q (2016).
19. A. E. Szymkowiak, R. L. Kelley, S. H. Moseley, and C. K. Stahle, "Signal processing for microcalorimeters," *J. Low Temp. Phys.* **93**, pp. 281-285, (1993).
20. H. Seta, et al., “The Digital Processing System for the Soft X-Ray Spectrometer Onboard Astro-H - The Design and the Performance,” *IEEE Transactions on Nuclear Science* **59**, pp. 366–372 (2012).
21. T. Hayashi, et al., “Point spread function of the Astro-H soft x-ray telescope (SXT),” *Proc. SPIE* **9905**, 99055D (2016).

22. M. E. Eckart, “Ground calibration of the Astro-H soft x-ray spectrometer,” *Proc. SPIE* **9905**, 99053W (2016)
23. M. Tsujimoto, et al., “In-orbit operation of the Astro-H SXS,” *Proc. SPIE* **9905**, 99050Y (2016).
24. F. S. Porter, et al., “In-flight performance of the soft x-ray spectrometer detector system on Astro-H,” *Proc. SPIE* **9905**, 99050W (2016).
25. M. A. Leutenegger, et al. “In-flight verification of the calibration and performance of the Astro-H soft x-ray spectrometer.” *Proc. SPIE* **9905**, 99053U (2016).
26. Hitomi Collaboration, *Nature*, **535**, 117, (2016).
27. C. A. Kilbourne, et al., “In-flight Calibration of Hitomi Soft X-ray Spectrometer (1) Background,” submitted to *Publications of the Astronomical Society of Japan* (2017).

Richard Kelley started out in X-ray astronomy as a graduate student at MIT using the SAS-3 satellite in the late 1970’s, and has participated in several X-ray observatories since coming to NASA/Goddard in 1983. He has mainly focused on the development of X-ray calorimeters and instruments for high-resolution spectroscopy. He has served as a member of the National Research Council Astro 2010 Decadal Survey Study Group on international partnerships, and was recently elected Fellow of the American Physical Society.

<u>Caption List</u>

Fig. 1 Schematic view of the Hitomi X-Ray Observatory[1]. The overall length of the 2700 kg observatory is 14 m. All of the x-ray mirrors are mounted on a fixed optical bench, but the Hard X-Ray Imager (HXI) is mounted on a deployable boom that extends 6 meters for a total focal length of 12 m. The mirror SXT-S focuses x-rays onto the SXS and has a 5.6 m focal length.

Fig. 2 Block diagram of the SXS instrument showing components, responsible agency, and interfaces.

Fig. 3 Schematic representation of the microcalorimeter array, showing 6 of the 36 pixels. The light gray area is ion-implanted Si to form the thermistor. The thermistor area is suspended by the four right-angle beams connected to the Si frame (dark gray). The four blue posts are made from a polymer that allows the HgTe absorbers (dark red) to be attached in a controlled manner using epoxy. The absorbers are 819 μm on a side, and the pixel-pixel pitch is 832 μm. These give a filling factor for the array of 97%. The absorbers are about 10 μm thick, and absorb > 98% of incident photons at 6 keV.

Fig. 4 The integrated SXS detector and ADR assembly being installed into the flight dewar in March 2014 at Sumitomo Heavy Industries, Japan.

Fig. 5 The installation of the high temperature super conducting (HTS) leads for ADR stages 1 and 2. The leads are protected by Kapton tubing, and these are attached to a T300 composite strong back that is custom formed for optimal placement in the dewar. The leads are terminated by bobbins that are mounted on the circuit board. These are use to make press-joints with the bobbins that are attached to the NbTi leads that go directly to the solenoid magnets.

Fig. 6 (Left) The efficiencies of key components of the SXS that determine the net throughput. (Right) Effective area of overall SXS instrument with the SXT. The black curve is the nominal end-end effective area while the blue curve shows the area with the aperture door closed. The aperture door has a Be window with a thickness of ~ 260 μm and a stainless steel protection screen.

Fig. 7 Functional block diagram of Xbox, the calorimeter amplifier, digitizer, and control unit.

Fig. 8 Functional block diagram of the ADR Controller (ADRC) and its interfaces to the internal dewar components.

Fig. 9 (Left) The response of the array to the ^{55}Fe calibration sources mounted on the Filter Wheel. The data were taken in orbit on 19 March 2016. (Right) Stacked spectra from the ^{55}Fe source, demonstrating an energy resolution of 4.9 eV.

Fig 10 Residual x-ray background over the 35 pixels in the field of view of the soft x-ray telescope. The background was obtained after applying the anticoincidence and standard data screening criteria.